JOURNAL OF GEOPHYSICAL RESEARCH, VOL. 96, NO. A7, PAGES 11,145–11,153, JULY 1, 1991

THE MAGNETIC BARRIER AT VENUS

T. L. Zhang, J. G. Luhmann, and C. T. Russell

Institute of Geophysics and Planetary Physics, University of California, Los Angeles

Abstract. The magnetic barrier at Venus is a region within which the magnetic pressure dominates all other pressure contributions. The barrier is formed in the inner region of the dayside magnetosheath to transfer solar wind momentum flux to the ionosphere. Passes through the dayside magnetosheath and ionopause with Pioneer Venus have allowed us to probe the magnetic barrier directly. These passes have been used to construct altitude profiles of the barrier. Here we define the ionopause as the lower boundary of the barrier. The upper boundary is defined as the altitude where the magnetosheath magnetic pressure is equal to half of the upstream solar wind dynamic pressure corrected by the boundary normal angle. The magnetic barrier is strongest at the subsolar point and weakens as expected with increasing solar zenith angle. The existence of a north-south asymmetry in the barrier strength is also demonstrated. The magnetic barrier is about 200 km thick at the subsolar point and 800 km thick at the terminator, which is comparable with the so-called "mantle." We find that the magnetic barrier transfers most of the solar wind dynamic pressure to the ionosphere via the enhanced magnetic pressure. The convected field gasdynamic model is found to predict the correct bow shock location if the magnetic barrier is treated as the obstacle.

Introduction

The interaction of the solar wind with solar system bodies can be divided into three categories. The simplest is the interaction with unmagnetized atmosphereless bodies such as the Moon, which directly absorbs the incident solar wind plasma. The second is the interaction with magnetized bodies whose large intrinsic magnetic fields stand off the solar wind flow (Mercury, Earth, Jupiter, Saturn, Uranus, and Neptune). The third is the interaction with highly conducting ionospheres. The solar wind interactions with Mars and Venus belong to this category.

The in situ measurements of the Pioneer Venus orbiter mission have improved our understanding of the ionosphere/solar wind interaction. The interaction between Venus and the solar wind has been described by many authors (cf. Russell and Vaisberg, 1983; Luhmann, 1986; Phillips and McComas, 1991). The highly electrically conducting ionosphere deflects the oncoming supersonic solar wind around the planet so that a bow shock is formed. The interaction of the postshock solar wind flow and ionosphere also results in a distinct boundary, the so-called ionopause. This ionopause separates the thermal plasma of the ionosphere from the hot magnetized plasma and magnetic field of the magnetosheath, which is defined as the region between ionopause and bow shock. Figure 1 illustrates the interaction of the solar wind with Venus. It also shows a magnetic barrier in the inner region of the magnetosheath. This barrier region is the subject of the present investigation.

Spreiter et al. [1966] predicted a density increase along the stagnation streamline from the bow shock to the magnetopause using a gasdynamic model. However, for an MHD flow such as the solar wind, Zwan and Wolf [1976] described another phenomenon. According to their analysis, the solar wind plasma upstream of a planetary obstacle is not continually compressed as it approaches the obstacle as for a gasdynamic flow, but is depleted of particles in the inner magnetosheath magnetic flux tubes. Thus, in their MHD treatment, a magnetic barrier is formed outside the obstacle boundary. This magnetic barrier transfers solar wind momentum flux to the obstacle via enhanced magnetic pressure.

Crooker et al. [1979] observed this plasma depletion in the Earth's magnetosheath at the dayside magnetopause using IMP 6 data. Russell et al. [1979] noticed a magnetic barrier at Venus in the early magnetic field and ionospheric plasma data returned by the Pioneer Venus orbiter (PVO). From other measurements on PVO, Spenner et al. [1980] identified a "mantle" region of reduced solar wind particle density containing some ionospheric photoelectrons where magnetic pressure dominated. At Mars, a similar boundary has been called the "ion cushion" by Vaisberg [1976] and the "planetopause" by Riedler et al. [1989]. Using PVO data, Vaisberg et al. [1980] showed that not all of the incident solar wind pressure was transferred by the magnetic barrier to the ionosphere of Venus. They found that plasma pressure might contribute approximately 1/4 to 1/3 of the total pressure within the magnetic barrier region. Figure 2 shows the qualitative magnetic barrier model devised by Russell and Vaisberg [1983] to describe the observation. In this model the magnetic field increases to a maximum in the magnetic barrier region while the density of ionospheric and solar wind plasma decreases to a minimum but is not necessarily totally depleted. The difference between the magnetic barriers at magnetic obstacles such as the Earth and atmospheric obstacles such as Venus and Mars is that ionospheric plasma may play a role in the latter.

In this paper the altitude profiles of the Venus magnetic barrier are derived from a statistical analysis of the PVO magnetometer data. The outer boundary of the magnetic barrier is then compared with the obstacle expected from gasdynamic models of the bow shock. The stagnation pressure is compared with that expected from gasdynamic theory. We find that ~83% of the upstream solar wind dynamic pressure appears as

Paper number 91JA00088.
0148-0227/91/91JA-00088$05.00

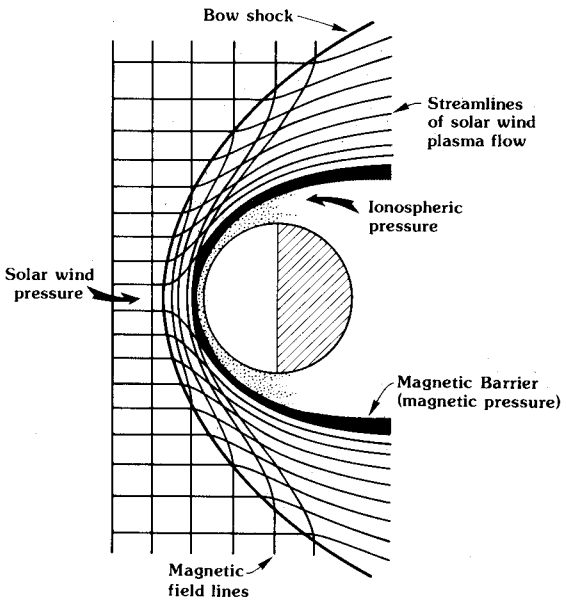

Fig. 1. The schematic of the Venus-solar wind interaction (not to scale), showing the magnetic barrier standing off the inflowing solar wind where the dynamic pressure equals the magnetic pressure. Thin lines show streamlines of solar flow, while the thick lines represent magnetic field in the plane of a perpendicular interplanetary field. The schematic also shows a magnetic barrier in the inner region of the magnetosheath.

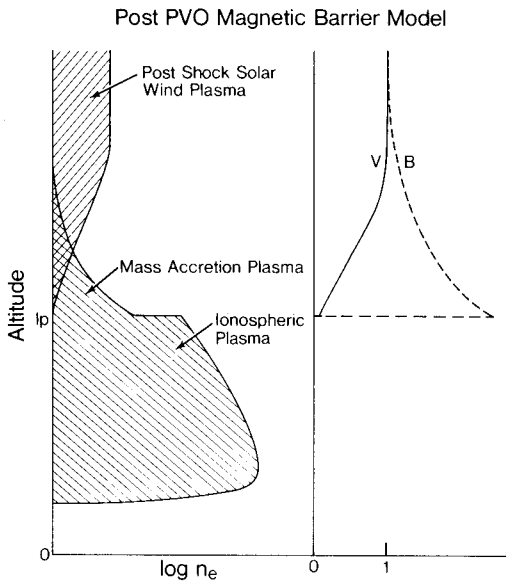

Fig. 2. Magnetic barrier model of Russell and Vaisberg [1983].

magnetic pressure in the barrier. We also find that gasdynamic theory provides a better approximation to the magnetosheath of Venus if it is assumed that the magnetic barrier instead of the ionopause is the obstacle.

Magnetic Barrier Observations

The data used for this study are the Pioneer Venus orbiter (PVO) measurements in the Unified Abstract Data System (UADS) file obtainable from National Space Science Data Center. These data consist of 12-s-averaged magnetic field component measurements for the period within ±30 min of periapsis together with the spacecraft position vectors. For this study, we used the first three seasons. After that time the spacecraft periapsis was above the ionopause. Also for the first three seasons, only dayside crossing orbits were used, or more precisely, orbits 134-234 in season 1, orbits 361-460 in season 2, and orbits 585-685 in season 3. Examples of this kind of data are shown in Figure 3. It can be seen that the magnetic field increases as the spacecraft approaches the planet. The maximum strength of the magnetic field depends on both the altitude and solar zenith angle (SZA). The magnetic data were binned in solar zenith angle and altitude to obtain statistical altitude profiles for the dayside magnetosheath.

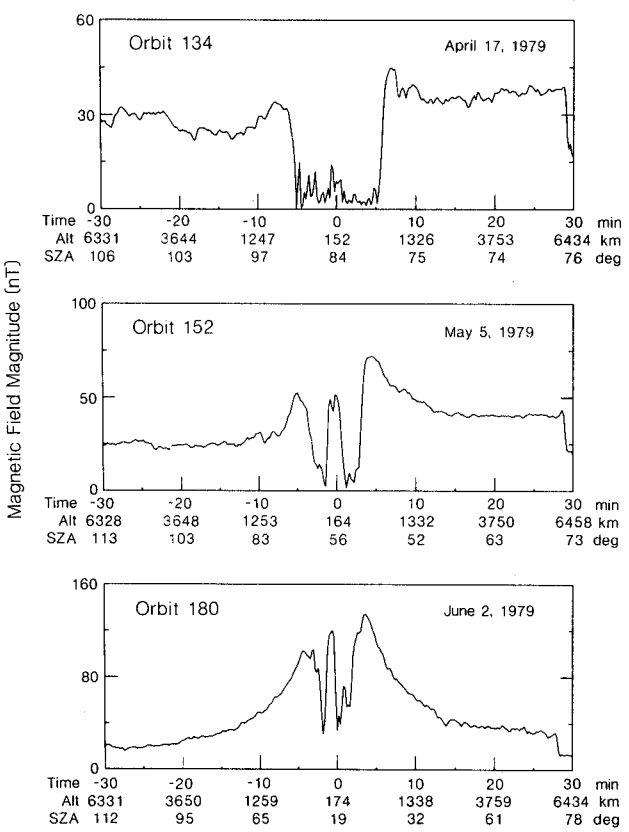

Fig. 3. Examples of time series of magnetic field magnitude observed at different solar zenith angles.

In this study, magnetic pressure data along each pass were normalized by upstream solar wind dynamic pressure. The solar wind data were provided by the Ames plasma analyzer (courtesy of A. Barnes, J. D. Mihalov, and P. Gazis). We selected relatively constant solar wind data on either inbound or outbound legs just outside the bow shock. Only a few orbits were not used in this study because of missing or uncertain solar wind data.

We calculate the pressure applied by the upstream solar wind using the formula $P_{sw} = K\rho v^2$,

where v is the solar wind speed, and ρ is the proton mass density, corrected for the average solar wind helium number abundance of 4-5%. The factor K is the solar wind pressure coefficient, 0.844-0.881, which we will later discuss theoretically.

Figure 4 shows normalized altitude profiles of median normalized magnetic pressure from the three PVO seasons. We normalized the altitude by the ionopause altitude of both inbound and outbound legs of each orbit using the formula

$$\text{normalized altitude} = \frac{\text{Alt}_{S/C} - \text{Alt}_{Ip}}{\text{Alt}_{Ip} + R_V}$$

where $\text{Alt}_{S/C}$ is spacecraft altitude at the time of the measurement and R_V is the radius of Venus. Here we used the ionopause position, Alt_{Ip}, defined by Phillips et al. [1988]. Figure 4 gives the profiles for different SZA intervals. For small solar zenith angles, 0°-30°, it can be seen that the normalized peak magnetic pressure is strongest. The normalized magnetic pressure reaches a maximum value of 0.61. For the "ideal" magnetic barrier model, the normalized magnetic pressure is expected to be near unity near the subsolar point. From our observations, the peak normalized magnetic pressure is 39% less than unity. One reason for this difference may be our data coverage, which is poor in the subsolar region due to PVO orbit characteristics. Second, we show medians of the data in a rather large range of SZA between 0° and 30° instead of at the subsolar point. Third, there may be a contribution of plasma pressure as suggested by Vaisberg et al. [1980], due to both hot solar wind plasma and ionospheric plasma in the magnetic barrier region. We will determine how much this contributes to magnetic barrier pressure later. Figure 4 also shows that in the intermediate SZA range, 30°-60°, the peak magnetic pressure is 0.40, and for high SZA, 60°-90°, the maximum is 0.19. It is clear that the magnetic barrier becomes weaker in strength and moves to higher altitudes as solar zenith angle increases. Another result shown in Figure 4 is that the slopes of the altitude profiles below the peak magnetic pressure are much steeper than the slopes above the peak. This implies that a large current density is concentrated in the region between the ionopause and the peak magnetic pressure point. In Figure 5, the data have been rotated according to the upstream transverse magnetic field direction and sorted into data sets representing the regions "north" and "south" of the magnetic draping "equator" as was done by Luhmann et al. [1985]. This analysis demonstrates that there is a north-south asymmetry of the normalized magnetic pressure profiles, which the authors attributed to

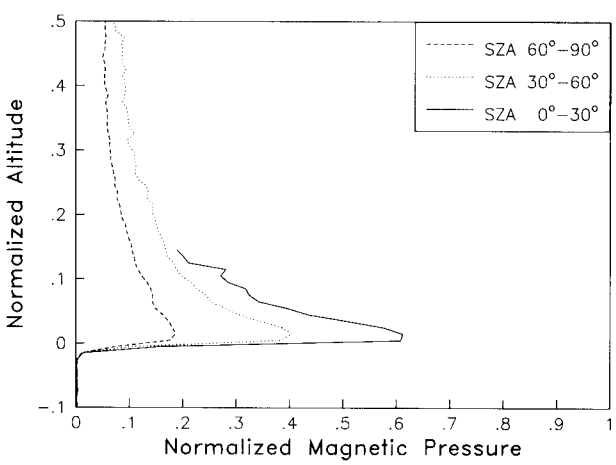

Fig. 4. Normalized altitude profiles of normalized magnetic pressure from the first three PVO seasons. The altitude is normalized by ionopause altitude. The magnetic pressure is normalized by upstream solar wind dynamic pressure. The upstream solar wind dynamic pressure has been corrected by two factors: the consideration of 4 to 5% of helium and the consideration of solar wind pressure coefficient K which is about 0.844 to 0.881.

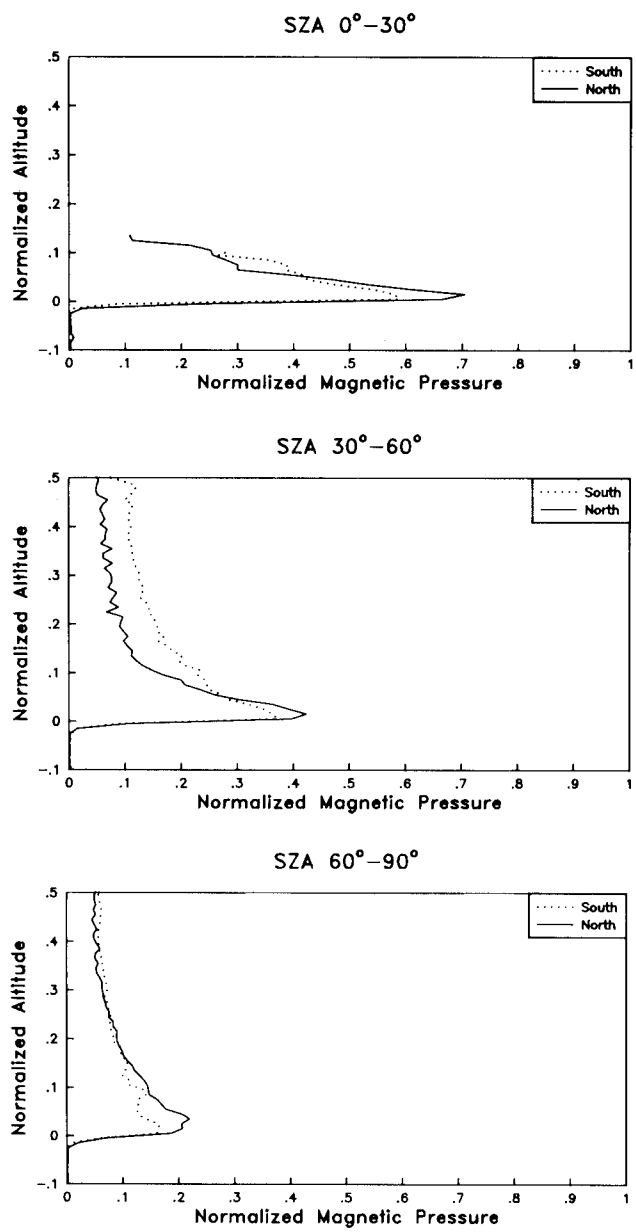

Fig. 5. North-south asymmetry of the magnetic barrier. See Figure 4 for further explanation.

the asymmetry in planetary ion pickup. However, the new hybrid models of the solar wind interaction, in which the ions are treated kinetically, show some asymmetry even in the absence of pickup ions [e.g., Brecht, 1990; Moore et al., 1991].

An alternative way to observe the magnetic barrier, or depletion layer, is by using plasma data. Although most of the time the PVO plasma analyzer cannot sample rapidly enough to resolve the depletion layer, there are occasional exceptions. Figure 6 shows plasma data from orbit 635, during which PVO passed just above the ionopause at a periapsis altitude of 317 km and SZA of 12.37°. In this pass, the plasma analyzer shows that near the ionopause there are depletions in plasma flux as expected in the barrier.

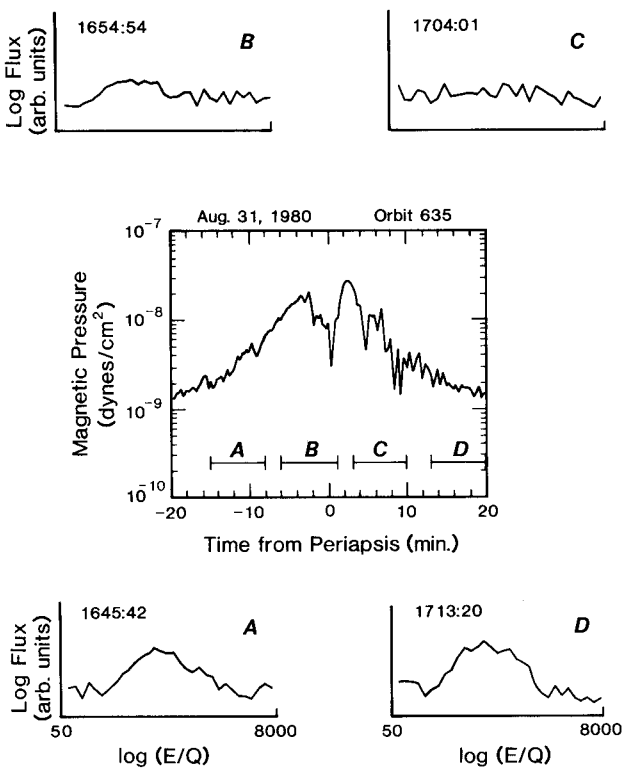

Fig. 6. Example of plasma depletion at the magnetic barrier region.

Size of Magnetic Barrier

The precise definition of the magnetic barrier should be related to the fact that it is a layer that is dominated by magnetic field. Zwan and Wolf [1976] defined the Earth's magnetic barrier as the region from the magnetopause up to where the postshock solar wind density is reduced by a factor of 2 or more. At that point, the thermal pressure drops a factor of $2^{5/3}$. They used an MHD numerical simulation to find out that the magnetic barrier, or depletion layer, is 700-1300 km thick in the subsolar region for Earth. By scaling their model calculations, they inferred that the magnetic barrier thickness is around 70-130 km for Venus.

The observational definition of the magnetic barrier thickness for Venus is rather difficult due to the lack of high-resolution plasma data in the postshock solar wind flow needed for the determination of the upper limit of the magnetic barrier. Therefore we define the magnetic barrier upper limit as the surface where the local magnetic pressure, $B^2/8\pi$, in the magnetosheath is equal to half of the upstream dynamic pressure adjusted for the barrier normal angle ψ, i.e., where $B^2/8\pi = \frac{1}{2}\rho v^2\cos^2\psi$. Figure 7 shows the altitude distribution of this upper magnetic barrier boundary as a function of SZA. Solid diamonds are the median altitudes for each of the SZA bins. There are only a few data points in the subsolar region due to the PVO trajectory, e.g., for the SZA bin of 0°-6°, only one data point was obtained. To estimate the altitude at the subsolar point, we find the best fit curve to the median altitudes. The depicted curve is the second-order polynomial fit:

$$\text{altitude} = 0.16 \times (\text{SZA})^2 - 0.55 \times (\text{SZA}) + 498$$

for altitude in kilometers and SZA in degrees, which has a correlation coefficient of 0.97. We have no physical reason to argue that the altitude should follow a polynomial function of SZA, but the correlation coefficient shows that the second-order polynomial is a good fit to the observations. According to this curve, the upper altitude of the barrier goes from ~500 km at the subsolar region to ~1700 km at the terminator. Figure 8 shows magnetic barrier upper boundary altitude as a function of upstream solar wind dynamic pressure. When the solar wind dynamic pressure is low (around 1 nPa), the magnetic barrier extends to 2000 km altitude, while when it is high (above 7 nPa), the upper boundary of the

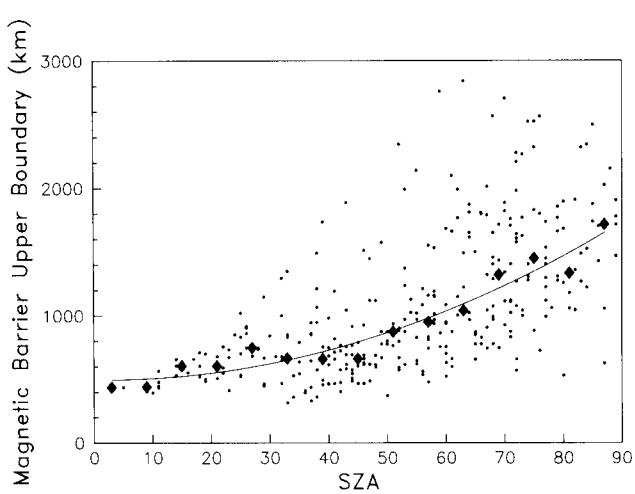

Fig. 7. Altitude distribution of the upper magnetic barrier boundary as a function of SZA. Here we define the magnetic upper boundary by equality of local magnetic pressure in the magnetosheath with half upstream dynamic pressure corrected by barrier normal angle. Solid diamonds are median altitudes of SZA bins. The small dots are individual measurements. The depicted curve is a second-order polynomial fit to the altitude-SZA median points.

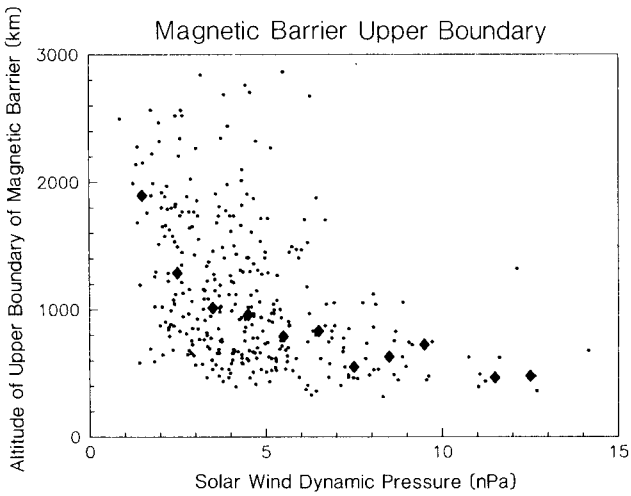

Fig. 8. Magnetic barrier upper boundary altitude as a function of upstream solar wind dynamic pressure.

magnetic barrier lies at about 600 km. The altitude of the peak magnetic pressure is shown as a function of SZA in Figure 9. The altitudes of this feature show less scatter than the upper magnetic barrier boundary. Their medians fit the curve

$$\text{altitude} = 0.11 \times (\text{SZA})^2 - 1.42 \times (\text{SZA}) + 382$$

with a correlation coefficient of 0.98. Figure 10 and Figure 11 show the altitude of the peak magnetic pressure as a function of upstream solar wind dynamic pressure and maximum magnetic pressure in the magnetic barrier, respectively. When the solar wind dynamic pressure increases, the altitude of the peak magnetic pressure decreases, reaching an asymptotic altitude of about 350 km. When this altitude is displayed versus the magnetic field pressure in the barrier, the same behavior is seen as expected but with much less scatter. We attribute the greater scatter in Figure 10 to the fact that the measurements of the solar wind pressure were made at a different time (tens of minutes to hours different) than the observation in the barrier.

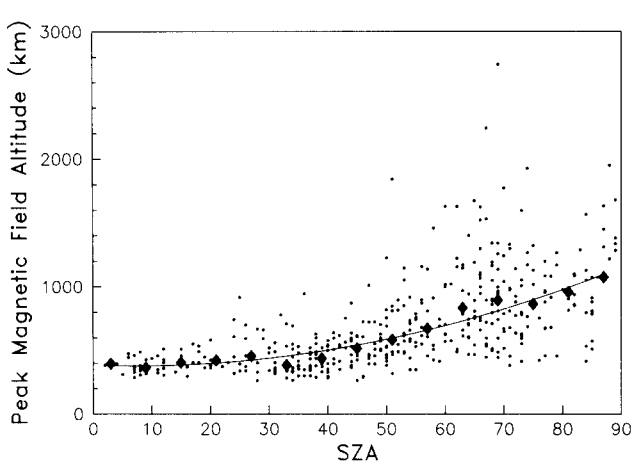

Fig. 9. The peak magnetic pressure altitude as a function of SZA.

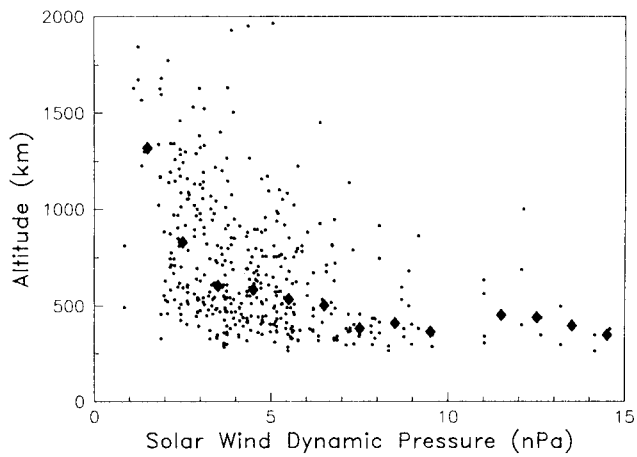

Fig. 10. The peak magnetic pressure altitude as a function of upstream solar wind dynamic pressure.

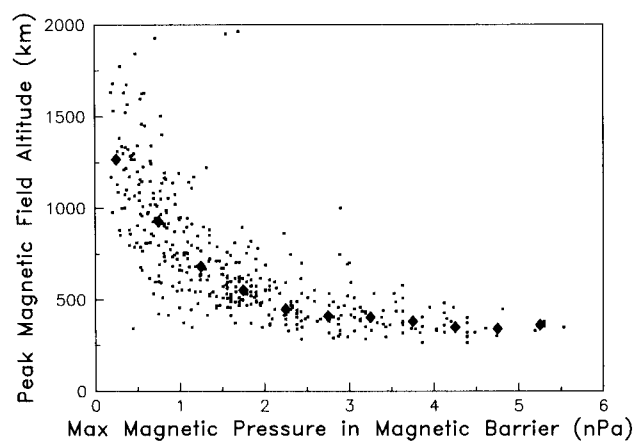

Fig. 11. The peak magnetic pressure altitude as a function of maximum magnetic pressure in the magnetic barrier.

Figure 12 compares the above boundaries with the ionopause defined by Phillips et al. [1988]. The ionopause fits the second-order polynomial:

$$\text{altitude} = 0.08 \times (\text{SZA})^2 - 0.12 \times (\text{SZA}) + 288$$

with a correlation coefficient of 0.98. Table 1 summarizes the results of the study of these different boundaries and features of the magnetic barrier.

Stagnation Pressure

The external gas pressure of the shocked solar wind on the obstacle, P_s, here taken to be the magnetic barrier, may be related to the upstream solar wind dynamic pressure $\rho_\infty v_\infty^2$ by a coefficient K defined by $K = p_s/\rho_\infty v_\infty^2 \cos^2\psi$. Here ψ is again the angle between the normal to the obstacle and the upstream solar wind direction. Thus ψ is zero at the nose and close to 90° near the terminator. Its precise value depends on the shape of the obstacle. Gasdynamic theory allows us to calculate K [Landau and Lifshitz, 1959].

We start with the continuity and Euler's equation for an ideal fluid with no viscosity or thermal conduction.

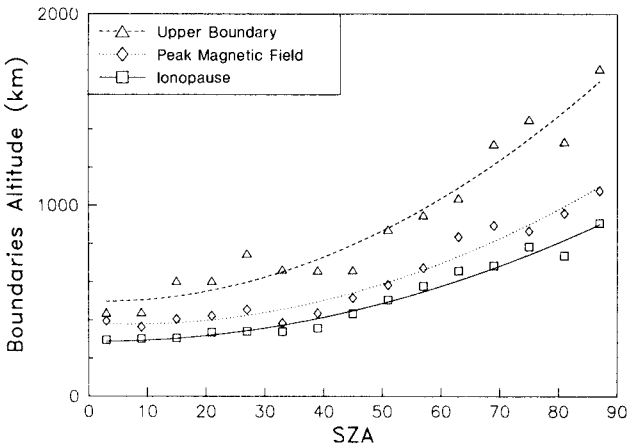

Fig. 12. Comparison of the altitude of the different boundaries of the magnetic barrier.

$$\frac{\partial \rho}{\partial t} + \nabla\cdot(\rho \mathbf{v}) = 0 \qquad (1)$$

$$\frac{\partial \mathbf{v}}{\partial t} + (\mathbf{v}\cdot\nabla)\mathbf{v} = -\frac{1}{\rho}\nabla p \qquad (2)$$

Thus the energy equation for an adiabatic fluid can be written as

$$p\rho^{-\gamma} = \text{const} \qquad (3)$$

where γ is the ratio of specific heats.

We first use the continuity equation and Euler's equation to estimate K qualitatively. Using equations (1) and (2), we obtain

$$\frac{\partial}{\partial t}(\rho \mathbf{v}) + \nabla\cdot(\rho \mathbf{v}\mathbf{v} + p\mathbf{I}) = 0 \qquad (4)$$

or in integral form

$$\frac{\partial}{\partial t}\int \rho \mathbf{v} dV = \oint (\rho \mathbf{v}\mathbf{v} + p\mathbf{I})\cdot \mathbf{n} S \qquad (5)$$

where

$$\rho \mathbf{v}\mathbf{v} + p\mathbf{I}$$

is called the momentum flow density tensor. The momentum flux through unit area in the direction of $\mathbf{n}$ can be written in the vector form:

$$\rho \mathbf{v}(\mathbf{v}\cdot\mathbf{n}) + p\mathbf{n}$$

If we assume a steady state, and we integrate equation (4) over the surface of a flow tube, we obtain the momentum conservation equation

$$(\rho v^2 + p)S = \text{const} \qquad (6)$$

where S is the area of the cross section of a flow tube. Considering a small flow tube around the stagnation streamline, we obtain

$$(\rho_\infty v_\infty^2 + p_\infty)S_\infty = (\rho_s v_s^2 + p_s)S_s \qquad (7)$$

where subscript ∞ refers to upstream parameters and s refers to the stagnation point. Near the stagnation point the condition $\rho_s v_s^2 \approx 0$ holds. Upstream in the solar wind, p_∞ is only around 1% of $\rho_\infty v_\infty^2$. So we can neglect p_∞. Also intuitively, we know that S_∞ is less than S_s. Therefore

$$K = \frac{p_s}{\rho_\infty v_\infty^2} = \frac{S_\infty}{S_s} < 1 \qquad (8)$$

Thus K is less than unity because of the divergence of the flow.

Now we derive a mathematical expression for K. From vector analysis,

$$\mathbf{v}\cdot\nabla\mathbf{v} = \tfrac{1}{2}\nabla v^2 - \mathbf{v}\times\nabla\times\mathbf{v}$$

We can combine equations (2) and (3) into

$$\frac{\partial \mathbf{v}}{\partial t} + \nabla\left(\frac{v^2}{2} + \frac{\gamma}{\gamma - 1}\frac{p}{\rho}\right) = \mathbf{v}\times\nabla\times\mathbf{v} \qquad (9)$$

for steady flow, $\partial \mathbf{v}/\partial t = 0$. The vector $\mathbf{v}\times\nabla\times\mathbf{v}$ is perpendicular to $\mathbf{v}$, so along a streamline:

Table 1. Magnetic Barrier Boundary Altitudes in Kilometers.

SZA Bin Center	Ionopause		Maximum Magnetic Pressure		Magnetic Barrier Upper Limit	
	n	Median	n	Median	n	Median
3	11	295.5	5	395.0	1	438.0
9	16	302.4	25	364.0	6	441.5
15	15	305.8	16	405.0	13	605.0
21	16	336.3	15	421.5	15	605.0
27	24	340.7	22	454.5	18	748.0
33	43	339.9	35	384.0	18	665.0
39	42	357.8	48	435.5	35	660.0
45	45	433.6	40	516.0	37	662.0
51	44	506.0	50	584.0	29	874.0
57	31	577.5	42	672.0	37	950.0
63	52	647.4	48	835.0	36	1039.0
69	56	684.5	64	894.5	49	1323.0
75	46	784.0	38	865.5	25	1451.0
81	53	736.9	22	958.5	22	1335.0
87	69	907.5	23	1076.0	17	1715.0

$$\frac{v^2}{2} + \frac{\gamma}{\gamma - 1}\frac{p}{\rho} = \text{const} \quad (10)$$

This is Bernoulli's equation for adiabatic flow. For an ideal gas,

$$p = \rho RT \quad (11)$$

where R is the gas constant and T is temperature, we can rewrite equation (10) in another form

$$\frac{v^2}{2} + \frac{\gamma}{\gamma - 1} RT = \text{const} \quad (12)$$

We recall that the sound speed is given by

$$c_s = (\gamma P/\rho)^{1/2} = (\gamma RT)^{1/2} \quad (13)$$

and the Mach number is

$$M^2 = \frac{v^2}{c_s^2} = \frac{v^2}{\gamma RT} = \frac{\rho v^2}{\gamma p} \quad (14)$$

We can then relate the stagnation pressure to the pressure of any point upstream along a streamline from equations (12), (3) and (11):

$$\frac{p_s}{p} = (1 + \frac{\gamma - 1}{2} M^2)^{\gamma/\gamma-1} \quad (15)$$

Because of the existence of the bow shock upstream of the obstacle, there is a jump in the different fluid parameters. Using the Rankine-Hugoniot equations, which consist of (6), (10), and the steady state form of (1), we have

$$\frac{p}{p_\infty} = 1 + \frac{2\gamma}{\gamma + 1}(M_\infty^2 - 1) \quad (16)$$

$$M^2 = \frac{1 + M_\infty^2 (\gamma-1)/2}{\gamma M_\infty^2 - (\gamma-1)/2} \quad (17)$$

where M_∞ and p_∞ are the Mach number and pressure upstream of the bow shock, and M and p the corresponding values downstream of the bow shock. Combining (14), (15), (16), and (17), we obtain

$$K = \frac{p_s}{\rho_\infty v_\infty^2} = (\frac{\gamma + 1}{2})^{(\gamma+1)/(\gamma-1)} \frac{1}{\gamma[\gamma - (\gamma-1)/2M_\infty^2]^{1/(\gamma-1)}} \quad (18)$$

K is 0.844 for $\gamma = 2$ and 0.881 for $\gamma = 5/3$ for hypersonic flow [cf. Spreiter et al., 1966]. If $\gamma = 5/3$ and $M = 4.5$, a more usual condition at Venus, K is 0.897. In summary then, in gasdynamic theory, K depends on Mach number and gamma, with gamma the more important factor.

Pressure Balance in the Magnetic Barrier

We have shown above that the normalized magnetic pressure in the barrier decreases with increasing solar zenith angle. From the viewpoint of the magnetic barrier model, the solar wind plasma interacts with the magnetic field of the magnetic barrier, which in turn acts on the ionospheric plasma. Of the total solar wind pressure, which is the sum of dynamic, plasma, and magnetic pressures, the dynamic pressure of the solar wind, ρv^2, which averages 5.5 nPa at Venus, contributes 98%. Thus the magnetic barrier pressure should balance solar wind dynamic pressure normal to the surface of the magnetic barrier. From the relation

$$p = K\rho_\infty v_\infty^2 \cos^2\psi \quad (19)$$

we expect the normalized magnetic barrier pressure to vary with the cosine squared of the magnetic barrier normal angle. Figure 13 shows the normalized maximum magnetic pressure medians in the magnetic barrier for 10° SZA bins. The barrier normal angle is calculated from the best second-order polynomial curve fit to the observed altitudes of maximum magnetic field.

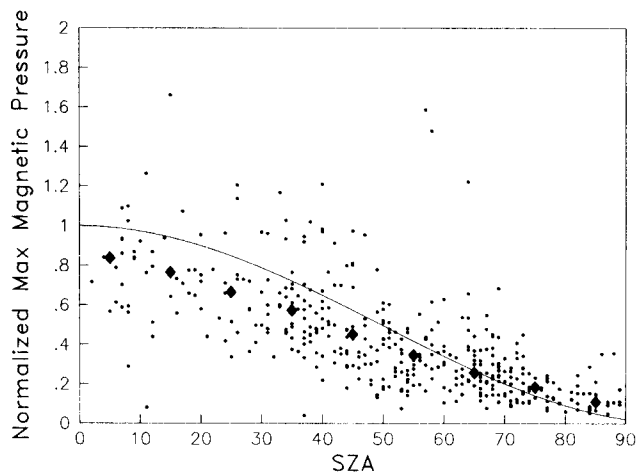

Fig. 13. The normalized maximum magnetic pressure as a function of SZA. Small dots are individual measurements. Diamonds are normalized maximum magnetic pressure medians at the magnetic barrier. The curve drawn is square of the cosine of the barrier normal angle which is calculated from the best fit second-order polynomial function of the observed altitude of maximum magnetic field as shown in Figure 9.

Figure 14 shows the normalized maximum magnetic pressure corrected by the cosine squared of the barrier normal angle as a function of SZA. Diamonds are medians binned by SZA. The straight line is the median line of the median points. This median gives a normalized maximum magnetic pressure in the barrier of 0.83. We attribute much of the scatter in Figures 13 and 14 to temporal variations in the solar wind between the time of the solar wind observations and the magnetic barrier measurements. These variations should create equal numbers of high and low points, with little effect on the median when statistical accuracy is high.

Discussion

One of the long-standing puzzles of the Venus bow shock comparisons with gasdynamic models has been the problem that the bow shock position implies that the obstacle is located above the ionopause [e.g., Slavin et al., 1980; Mihalov et al., 1982]. This study reconciles observations with the gasdynamic calculation by showing that the altitude of the barrier is the altitude of the effective obstacle which produced the correct bow

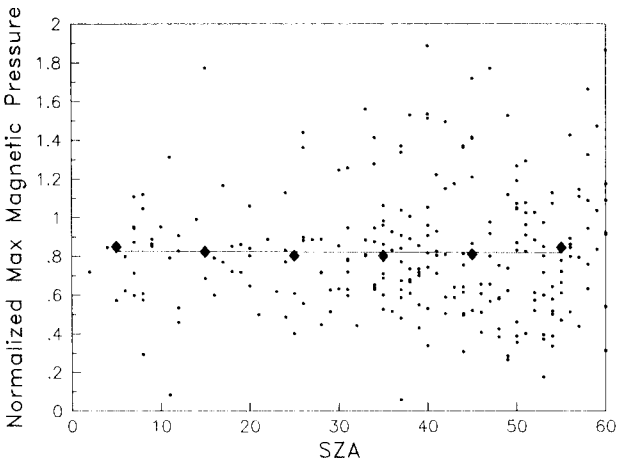

Fig. 14. The normalized maximum magnetic pressure corrected by the square of the cosine of the barrier normal angle as a function of SZA. Diamonds are medians binned by SZA. The straight line is the median of the medians in each bin.

shock position in earlier studies [Zhang et al., 1990]. The gasdynamic models as formulated to date do not create a magnetic barrier. Thus to optimize their predictions of shock location and flow field we must presently introduce the magnetic barrier on an ad hoc basis. Other numerical models such as the hybrid models of Brecht [1990] and Moore et al. [1991] can and do produce magnetic barriers, but are much more expensive to compute.

It should be noted that in reality the magnetic barrier builds up gradually and is not an impenetrable "surface" in the magnetosheath. Thus there is no well-defined point to choose at the top of the magnetic barrier in contrast to the ionopause location, which is usually well-defined. Our choice of the point where the magnetic pressure is half the total expected pressure has some arbitrariness to it. Ideally one would like to compare these barrier measurements with either a global MHD magnetosheath model or hybrid model in which the physical processes formed by the barrier were included.

The fact that the bow shock position shows a solar cycle variation implies that the magnetic barrier also varies. We were not able to study the magnetic barrier at solar minimum due to the evolution of the PVO orbit. The fact that the shock was more distant during solar maximum, when the data used in the present study were obtained, than at solar minimum implies that the magnetic barrier is thicker at solar maximum than it is at solar minimum.

Conclusions

Using a statistical data base of Pioneer Venus orbiter magnetometer and solar wind data, we have obtained altitude profiles of the magnetic pressure in the subsolar magnetosheath and compared them with the incident solar wind dynamic pressure. We find that the maximum magnetic field in the magnetosheath accounts for ~83% of the incident solar wind dynamic pressure, which is close to that expected if there is little or no plasma in the magnetic barrier. If one defines the top of the magnetic barrier as the altitude where the magnetosheath magnetic pressure is equal to one half of the upstream solar wind dynamic pressure, one obtains a boundary that is at ~500 km altitude at the subsolar point and ~1700 km at the terminator. The obstacle defined by this surface produces a gasdynamic model bow shock position in better accord with the observations than that produced with an obstacle located at the ionopause, but this definition of the obstacle is in some sense an ad hoc correction of the model. Magnetohydrodynamic and hybrid models of the magnetosheath are expected to better reproduce the observed bow shock location and the structure of the magnetosheath.

Acknowledgments. This work was supported by the National Aeronautics and Space Administration under research grant NAG2-501.

The Editor thanks one referee for his assistance in evaluating this paper.

References

Brecht, S. H., Magnetic asymmetries of unmagnetized planets, Geophys. Res. Lett., 17, 1243, 1990.

Crooker, N. U., T. E. Eastman, and G. S. Stiles, Observations of plasma depletion in the magnetosheath at the dayside magnetopause, J. Geophys. Res., 84, 869-874, 1979.

Landau, L. D., and E. M. Lifshitz, Fluid Mechanics, Addison-Wesley, Reading, Mass., 1959.

Luhmann, J. G., The solar wind interaction with Venus, Space Sci. Rev., 44, 241-306, 1986.

Luhmann, J. G., C. T. Russell, J. R. Spreiter, and S. S. Stahara, Evidence for mass-loading of the Venus magnetosheath, Adv. Space Res., 5, 307-311, 1985.

Mihalov, J. D., J. R. Spreiter and S. S. Stahara, Comparison of gasdynamic model with steady solar wind flow around Venus, J. Geophys. Res., 87, 10,363-10,371, 1982.

Moore, K., R. V. Thomas, and D. J. McComas, Global hybrid simulation of the solar wind interaction with the dayside of Venus, J. Geophys. Res., 96, 7779-7791, 1991.

Phillips, J. L., and D. J. McComas, The magnetosheath and magnetotail of Venus, Space Sci. Rev., 55, 1-80, 1991.

Phillips, J. L., J. G. Luhmann, W. C. Knudsen, and L. H. Brace, Asymmetries in the location of the Venus ionopause, J. Geophys. Res., 93, 3927-3941, 1988.

Riedler, W., et al., Magnetic fields near Mars: First results, Nature, 341, 604-67, 1989.

Russell, C. T., and O. Vaisberg, The interaction of the solar wind with Venus, in Venus, edited by D. M. Hunten, L. Colin, T. M. Donahue, and V. I. Moroz, pp. 873-940, University of Arizona Press, Tucson, 1983.

Russell, C. T., R. C. Elphic, and J. A. Slavin, Initial Pioneer Venus magnetic field results: Dayside observations, Science, 203, 745-748, 1979.

Slavin, J. A., R. C. Elphic, C. T. Russell, F. L. Scarf, J. H. Wolfe, J. D. Mihalov, D. S. Intriligator, L. H. Brace, H. A. Taylor, Jr., and R. E. Daniell, Jr., The solar wind interaction with Venus: Pioneer Venus

observation of bow shock location and structure, J. Geophys. Res., 85, 7625-7641, 1980.

Spenner, K., W. C. Knudsen, K. L. Miller, V. Novak, C. T. Russell, and R. C. Elphic, Observation of the Venus mantle, the boundary region between solar wind and ionosphere, J. Geophys. Res., 85, 7655-7662, 1980.

Spreiter, J. R., A. L. Summers, and A. Y. Alksne, Hydromagnetic flow around the magnetosphere, Planet. Space Sci., 14, 223-253, 1966.

Vaisberg, O. L. et al., Mars-plasma environment, in Physics of Solar Planetary Environments, vol 2, edited by D. J. Williams, pp. 854-871, AGU, Washington, D. C., 1976.

Vaisberg, O. L., D. S. Intriligator and V. N. Smirnov, An empirical model of the Venusian outer environment 1, The slope of the dayside solar wind - atmosphere interface, J. Geophys. Res., 85, 7643-7650, 1980.

Zhang, T. L., J. G. Luhmann, and C. T. Russell, The solar cycle dependence of the location and shape of the Venus bow shock, J. Geophys. Res., 95, 14,961-14,968, 1990.

Zwan, B. J., and R. A. Wolf, Depletion of solar wind plasma near a planetary boundary, J. Geophys. Res., 81, 1636-1648, 1976.

J. G. Luhmann, C. T. Russell, and T. L. Zhang, Institute of Geophysics and Planetary Physics, University of California, Los Angeles, CA 90024.

(Received November 12, 1990;
revised January 2, 1991;
accepted January 2, 1991.)